TUDelft

Delft University of Technology

Thickness-weighted averaging in tidal estuaries and the vertical distribution of the eulerian residual transport

Klingbeil, Knut; Becherer, Johannes; Schulz, Elisabeth; de Swart, Huib E.; Schuttelaars, Henk M.; Valle-Levinson, Arnoldo; Burchard, Hans

Important note
To cite this publication, please use the final published version (if applicable).
Please check the document version above.

Thickness-Weighted Averaging in Tidal Estuaries and the Vertical Distribution of the Eulerian Residual Transport

KNUT KLINGBEIL,[a,b] JOHANNES BECHERER,[c] ELISABETH SCHULZ,[b] HUIB E. DE SWART,[d]
HENK M. SCHUTTELAARS,[e] ARNOLDO VALLE-LEVINSON,[f] AND HANS BURCHARD[b]

[a] *Department of Mathematics, University of Hamburg, Hamburg, Germany*
[b] *Leibniz Institute for Baltic Sea Research Warnemünde (IOW), Rostock, Germany*
[c] *College of Earth, Ocean, and Atmospheric Sciences, Oregon State University, Corvallis, Oregon*
[d] *Department of Physics, Institute for Marine and Atmospheric Research Utrecht, Utrecht University, Utrecht, Netherlands*
[e] *Delft Institute of Applied Mathematics, Delft University of Technology, Delft, Netherlands*
[f] *Department of Civil and Coastal Engineering, University of Florida, Gainesville, Florida*

ABSTRACT

This paper presents thickness-weighted averaging (TWA) in generalized vertical coordinates as a unified framework for a variety of existing tidal-averaging concepts in seas and estuaries. Vertical profiles of resulting residual quantities depend on the specific vertical coordinate, which is held fixed during the averaging process. This dependence is demonstrated through the application to one-dimensional analytical tidal flow with sediment transport, to field observations from a tidal channel, and to model results from a two-dimensional estuary. The use of different coordinate systems provides complementary views on the residual dynamics and stresses the importance of a correct interpretation of residual quantities obtained by tidal averaging.

1. Introduction

Tidal averaging is commonly used to unravel the underlying residual dynamics in coastal systems dominated by oscillating tidal flows. Residual averages can be obtained in different coordinate systems with the corresponding spatial coordinates held fixed during the averaging process. The two most intuitive cases are Eulerian and Lagrangian averaging. The Eulerian average describes the mean state at a fixed position, or equivalently the mean property of all fluid parcels when passing this single position. In contrast, the Lagrangian average describes the mean property of an individual parcel (defined by fixed material coordinates) along its trajectory and can be referenced to the mean position of this parcel [see Generalized Lagrangian Mean theory of Andrews and McIntyre (1978)]. All other types of averaging are a mixture of these two cases. This mixture can be prone to misinterpretation, because the averages are neither associated to a single fixed position nor to a single fluid parcel.

To reduce complexity, the present study considers averages obtained at a fixed horizontal position with

coordinates (x, y) and at a fixed generalized vertical coordinate $s(x, y, z, t)$, which can be associated with a varying vertical position z. This horizontally Eulerian framework fits reasonably well with analytical studies, and covers various sampling and discretization techniques applied in instrumentation and modeling. In the context of tidal averaging there is an ongoing debate about the preferred vertical coordinate. In geopotential coordinates z levels can become void of water during the course of a tidal cycle, which requires some special treatment for averaging. Therefore, Kjerfve (1975) suggested to average in surface-following σ coordinates instead, that is, at fixed levels of $\sigma = (z - \eta)/D$, with D and η being the total water depth and the oscillating position of the free surface, respectively. Alternatively, Walin (1977) and MacCready (2011) developed an isohaline framework to investigate residual dynamics with respect to salinity classes. It is evident that the choice of vertical coordinate depends on the specific purpose of investigation. Besides the correct interpretation of residual quantities in the chosen coordinate space, another difficulty originates from the direct application of a temporal low-pass filter. In general, the direct application does not result in conservative residual quantities, that is, residuals that are consistent with

Corresponding author: Knut Klingbeil, knut.klingbeil@io-warnemuende.de

conservation of mass or momentum. This was already noted by Kjerfve (1975) for the velocity in σ coordinates, in the following denoted by u^σ. Therefore, Giddings et al. (2014) argued for the use of a rescaled velocity $u_M^\sigma = Du^\sigma/\langle D \rangle$ that includes the residual water depth $\langle D \rangle$. For depth-averaged studies the problem was solved by the introduction of the Eulerian residual transport velocity by Zimmerman (1979). Still missing is an extension to depth-dependent quantities in a generalized vertical coordinate.

Furthermore, in the literature, the presentation of residual quantities can be confusing because sometimes the nomenclature is inaccurate (e.g., labeling of residuals as being Eulerian or Lagrangian) or inconsistent (e.g., the use of the term *transport velocity*), definitions are not precise, or the data processing is unclear (e.g., the coordinate system). But this clarity and accuracy is required for a correct interpretation of the results.

The aim of this paper is to reduce confusion and complexity by presenting the concept of thickness-weighted averaging (TWA) as a unified approach to calculate conservative tidally averaged quantities in any vertical coordinate system. TWA was originally developed for the parameterization of eddy-induced transports in isopycnal coordinates (e.g., de Szoeke and Bennet 1993; McDougall and McIntosh 2001; Greatbatch and McDougall 2003; Young 2012, and references therein), and later was also used to derive the governing equations describing the 3D interaction of currents and surface gravity waves (Aiki and Greatbatch 2012, 2013, 2014). In this paper the concept of TWA is extended to a generalized vertical coordinate and to depth-averaged quantities. The coordinate transformation is explained in section 2a. In section 2b the commutativity of TWA and depth-averaging is discussed as a necessary condition for conservative residuals. Section 2c extends the original TWA concept to nonmonotonic coordinate functions $s(z)$ and shows the relation to the so-called Total Exchange Flow (TEF) analysis of MacCready (2011). Section 3 demonstrates the dependence of vertical profiles of resulting residual quantities on the averaging operator and on the specific vertical coordinate, which is held fixed during the averaging process. Results are shown for one-dimensional analytical tidal flow, for field observations from a tidal channel, and for a numerical model of a two-dimensional estuary. A discussion and final conclusions are given in section 4 and section 5, respectively. Appendix A outlines the application of the TWA operator to the governing 3D equations. The procedure of TWA for discrete data is explained in appendix B. Appendix C provides details about the analytical solution for one-dimensional tidal flow with sediment transport.

2. Thickness-weighted averaging

a. Vertical coordinate transformation

The TWA concept was originally developed for density coordinates in a stably stratified ocean. It is straightforward to extend the original concept to a generalized vertical coordinate $s(x, y, z, t)$ that is strictly monotonic in z (further generalization of the TWA concept to nonmonotonic functions $s(z)$ is presented in section 2c). With this constraint there exists a well-defined coordinate transformation to the inverse function $z(s)$ with a nonzero, single-signed Jacobian $\partial z/\partial s$. More details and examples of vertical coordinate transformations are given in Kasahara (1974) and in Burchard and Petersen (1997). Besides the monotonicity constraint, the generalized vertical coordinate is completely arbitrary and thus cannot be categorized as being Eulerian ($s = z$, i.e., geopotential coordinates) or vertically Lagrangian ($\dot{s} = Ds/Dt = 0$, i.e., vertically following a coordinate-specific material surface). The use of misleading terms like semi-Eulerian framework is explicitly discouraged here in favor of the precise term horizontally Eulerian framework. If not obvious from the context, the functional dependence of a quantity ψ within a specific coordinate system is indicated by its superscript, for example, $\psi^z(x, y, z, t)$. For brevity, the superscript s for the functional dependence on the generalized vertical coordinate s is usually omitted.

b. Conservative averaging

The governing equations (see appendix A) are only valid inside the water column, that is, between the bottom at $z = -H(x, y)$ and the free surface at $z = \eta(x, y, t)$. To simplify the definition of averages in terms of integrals formally also including samples outside the water column, any instantaneous quantity ψ has to be masked outside the water column. Below the bottom ($z < -H$) and above the free surface ($\eta < z$) all data are defined to be zero ($\psi \equiv 0$). This masking is also transferred to transformed spaces and allows obtaining tidal averages in any coordinate system with a temporal low-pass filter, in the following denoted by angle brackets $\langle \cdot \rangle$, and for example given by a simple running mean over (tidal) period T:

$$\langle \psi \rangle(x, y, s, t) = \frac{1}{T}\int_{t-T/2}^{t+T/2} \psi(x, y, s, t')\, dt'. \qquad (1)$$

Considering the masking described above, the depth-average operator, denoted by square brackets $[\cdot]$, can be defined for an instantaneous quantity as

$$[\psi] = \frac{1}{D}\int_{-H}^{\eta} \psi^z\, dz = \frac{1}{D}\int_{-\infty}^{+\infty} \left|\frac{\partial z}{\partial s}\right| \psi^s\, ds, \qquad (2)$$

with $|\partial z/\partial s|$ being the differential thickness, given by the Jacobian of the coordinate transformation. The depth-averaged velocity $U = [u]$, with u being the depth-dependent velocity, can also be interpreted as a transport velocity when written as $U = M/D$, with the depth-integrated transport

$$M = \int_{-H}^{\eta} u \, dz. \tag{3}$$

The Eulerian residual transport $\langle M \rangle$ cannot be obtained in terms of the residual velocity $\langle U \rangle$ due to additional correlations with the water depth: $\langle M \rangle = \langle DU \rangle \neq \langle D \rangle \langle U \rangle$. In contrast, the Eulerian residual transport velocity (Zimmerman 1979),

$$\hat{U} = \frac{\langle M \rangle}{\langle D \rangle} = \frac{\langle DU \rangle}{\langle D \rangle}, \tag{4}$$

by definition "conserves" $\langle M \rangle = \langle D \rangle \hat{U}$ and is the residual velocity associated with the balance of momentum under the Boussinesq approximation [also see (A11)]. Furthermore, with the depth average operator for tidally averaged quantities [different from the operator for instantaneous quantities in (2)],

$$[\langle \psi \rangle] = \frac{1}{\langle D \rangle} \int_{-\infty}^{+\infty} \left\langle \left| \frac{\partial z}{\partial s} \right| \right\rangle \langle \psi \rangle \, ds, \tag{5}$$

it can be shown that, except for geopotential coordinates, the residual velocity profile $\langle u \rangle$ does not conserve $\langle M \rangle$ because $[\langle u \rangle] \neq \hat{U}$. However, aiming at physical interpretation, also the profiles of residual quantities should be conservative, that is, consistent with conservation of mass or momentum. Since the direct application of the temporal low-pass filter (1) is not conservative, neither for depth-averaged nor for depth-dependent velocities, an alternative averaging operator is needed. Interpreting the hat symbol of $\hat{U}$ as an operator, an appropriate averaging operator for depth-averaged quantities can be deduced from (4):

$$\widehat{[\psi]} = \frac{\langle D[\psi] \rangle}{\langle D \rangle}. \tag{6}$$

The question is how to extend this conservative operator to depth-dependent quantities in order to yield a residual velocity profile $\hat{u}$ such that $[\hat{u}] = \hat{U} = \widehat{[u]}$, with the depth average of $\hat{u}$ being defined in analogy to (5):

$$[\hat{\psi}] = \frac{1}{\langle D \rangle} \int_{-\infty}^{+\infty} \left\langle \left| \frac{\partial z}{\partial s} \right| \right\rangle \hat{\psi} \, ds. \tag{7}$$

With (2), (6), and (7) the required commutativity of operators can be written as

$$\widehat{[\psi]} \overset{(6),(2)}{=} \frac{\left\langle D \left(\frac{1}{D} \int_{-\infty}^{+\infty} \left| \frac{\partial z}{\partial s} \right| \psi \, ds \right) \right\rangle}{\langle D \rangle}$$

$$= \frac{1}{\langle D \rangle} \int_{-\infty}^{+\infty} \left\langle \left| \frac{\partial z}{\partial s} \right| \right\rangle \left(\frac{\left\langle \left| \frac{\partial z}{\partial s} \right| \psi \right\rangle}{\left\langle \left| \frac{\partial z}{\partial s} \right| \right\rangle} \right) ds$$

$$\overset{(7)}{=} \left[\frac{\left\langle \left| \frac{\partial z}{\partial s} \right| \psi \right\rangle}{\left\langle \left| \frac{\partial z}{\partial s} \right| \right\rangle} \right] \equiv [\hat{\psi}], \tag{8}$$

and the conservative averaging operator for depth-dependent quantities can be deduced as

$$\hat{\psi} = \frac{\left\langle \left| \frac{\partial z}{\partial s} \right| \psi \right\rangle}{\left\langle \left| \frac{\partial z}{\partial s} \right| \right\rangle}. \tag{9}$$

For isopycnal coordinates ($s = \rho$) the operator in (9) is identical to the classical TWA defined by de Szoeke and Bennet (1993). This nomenclature will be adopted for (9) and (6). For depth-averaged quantities in (6) the associated thickness is given by the total water depth D, whereas for depth-dependent quantities in (9) it is given by the differential thickness $|\partial z/\partial s|$. Despite being different mathematical operators, the hat symbol is used in both cases because from the context it is always obvious whether the TWA operator is applied to depth-averaged or depth-dependent quantities. The same holds for the depth-averaging operator in (2), (5), and (7), applied either to instantaneous or residual quantities. The vertical integral of residual quantities in (5) and (7) is always normalized by the residual water depth $\langle D \rangle$, also for residual quantities with nonzero values at mean vertical levels above $\langle \eta \rangle$, for example, for residual quantities in geopotential coordinates. An overview of all operators in continuous space and for discrete data is given in Table 1.

Related to the properties discussed above, the TWA defined in (9) shows further useful aspects:

(i) By definition the TWA takes into account the correlation with the Jacobian, therefore no additional covariance terms appear in the low-pass-filtered governing equations in generalized vertical coordinates [see (A9)].

(ii) For σ coordinates the Jacobian is given by $\partial z/\partial s = D$, and the TWA velocity $\hat{u}^{\sigma}$ naturally recovers $\langle u_M^{\sigma} \rangle$ used by Giddings et al. (2014), without the need to define the (unphysical) intermediate velocity $u_M^{\sigma} = D u^{\sigma}/\langle D \rangle$.

(iii) With $\widehat{[\psi]}$ being independent of the original vertical coordinate system, the commutativity relation (8)

TABLE 1. Overview of averaging operators. The arbitrary quantity ψ is masked outside the water column. For geopotential and σ coordinates the Jacobians are given by $\partial z/\partial s = 1$ and $\partial z/\partial s = D$, respectively, with D being the total water depth. Discrete data $\psi^n_{(l)}$ are given for l_{max} bins with bin thickness $D^n_{(l)}$. Indices l and n denote the bin and the time stage, respectively. For simplicity the N time stages are assumed to be sampled with constant frequency. Terms $D^n_{(l)}\psi^n_{(l)}$ and $\langle D_{(l)}\psi_{(l)}\rangle$ are the instantaneous and mean content of ψ in the bin. In Finite-Volume model codes layer heights and the prognostic layer-averaged variables can be directly used as $D^n_{(l)}$ and $\psi^n_{(l)}$, which is a special case of (B2b) and (B5) in appendix B.

	Reference	Operator in continuous space	Operator for discrete data
Unweighted average	(1)	$\langle\psi\rangle = \dfrac{1}{T}\displaystyle\int_{t-T/2}^{t+T/2}\psi(t')\,dt'$	$\langle\psi_{(l)}\rangle = \dfrac{1}{N}\displaystyle\sum_{n=1}^{N}\psi^n_{(l)}$
TWA	(9)	$\hat\psi = \dfrac{\left\langle\left\lvert\frac{\partial z}{\partial s}\right\rvert\psi\right\rangle}{\left\langle\left\lvert\frac{\partial z}{\partial s}\right\rvert\right\rangle}$	$\hat\psi_{(l)} = \dfrac{\langle D_{(l)}\psi_{(l)}\rangle}{\langle D_{(l)}\rangle}$
Depth average	(2)	$[\psi] = \dfrac{1}{D}\displaystyle\int_{-\infty}^{+\infty}\left\lvert\frac{\partial z}{\partial s}\right\rvert\psi\,ds$	$[\psi^n] = \dfrac{\sum_{l=1}^{l_{max}} D^n_{(l)}\psi^n_{(l)}}{\sum_{l=1}^{l_{max}} D^n_{(l)}}$
Combinations	(5)	$[\langle\psi\rangle] = \dfrac{1}{\langle D\rangle}\displaystyle\int_{-\infty}^{+\infty}\left\langle\left\lvert\frac{\partial z}{\partial s}\right\rvert\right\rangle\langle\psi\rangle\,ds$	$[\langle\psi\rangle] = \dfrac{\sum_{l=1}^{l_{max}}\langle D_{(l)}\rangle\langle\psi_{(l)}\rangle}{\sum_{l=1}^{l_{max}}\langle D_{(l)}\rangle}$
	—	$\langle[\psi]\rangle = \left\langle\dfrac{1}{D}\displaystyle\int_{-\infty}^{+\infty}\left\lvert\frac{\partial z}{\partial s}\right\rvert\psi\,ds\right\rangle$	$\langle[\psi]\rangle = \left\langle\dfrac{\sum_{l=1}^{l_{max}} D_{(l)}\psi_{(l)}}{\sum_{l=1}^{l_{max}} D_{(l)}}\right\rangle$
	(7)	$[\hat\psi] = \dfrac{1}{\langle D\rangle}\displaystyle\int_{-\infty}^{+\infty}\left\langle\left\lvert\frac{\partial z}{\partial s}\right\rvert\right\rangle\hat\psi\,ds$	$[\hat\psi] = \dfrac{\sum_{l=1}^{l_{max}}\langle D_{(l)}\psi_{(l)}\rangle}{\sum_{l=1}^{l_{max}}\langle D_{(l)}\rangle}$
	(6)	$\widehat{[\psi]} = \dfrac{\langle D[\psi]\rangle}{\langle D\rangle}$	$\widehat{[\psi]} = \dfrac{\left\langle\sum_{l=1}^{l_{max}} D_{(l)}\psi_{(l)}\right\rangle}{\left\langle\sum_{l=1}^{l_{max}} D_{(l)}\right\rangle}$

shows that this independence now also holds for the depth-averaged TWA $[\hat\psi]$. This expected property of depth-averaged residuals does not hold for the depth-averaged unweighted residual $[\langle\psi\rangle]$. An overview of the commutativity properties in different vertical coordinate systems is given in Table 2.

The operators listed in Table 1 can be extended to higher dimensions to support cross-sectional and volume averages. Replacing the vertical integrals either by cross-sectional or volume integrals, the depth D by either the cross-sectional area A or the volume V, and the Jacobian of the vertical coordinate transformation $\partial z/\partial s$ by the Jacobian of the corresponding higher-dimensional transformation, for example, $\partial(x, z)/\partial(\xi, s)$, gives consistent operators that still guarantee conservativity and commutativity. For example, in analogy to (8), the conservative residual cross-sectional average in the x–z plane reads

$$\frac{\left\langle A\left(\frac{1}{A}\iint\psi\,dA\right)\right\rangle}{\langle A\rangle} = \frac{\left\langle A\left(\frac{1}{A}\iint\left\lvert\frac{\partial(x,z)}{\partial(\xi,s)}\right\rvert\psi\,d\xi\,ds\right)\right\rangle}{\langle A\rangle} = \frac{1}{\langle A\rangle}\iint\left\langle\left\lvert\frac{\partial(x,z)}{\partial(\xi,s)}\right\rvert\right\rangle\left(\frac{\left\langle\left\lvert\frac{\partial(x,z)}{\partial(\xi,s)}\right\rvert\psi\right\rangle}{\left\langle\left\lvert\frac{\partial(x,z)}{\partial(\xi,s)}\right\rvert\right\rangle}\right)d\xi\,ds, \qquad (10)$$

with ξ being the optionally transformed coordinate in the x direction. Conservative residual cross-sectional averages in σ coordinates were presented by Dronkers and van de Kreeke (1986) and Lerczak et al. (2006).

TABLE 2. Commutativity of averaging operators in different vertical coordinate systems. The operators are defined in Table 1. The first row shows the general operator relations in an arbitrary vertical coordinate (i.e., the generalized vertical coordinate s), whereas the second and third rows show the special cases of σ and z coordinates, respectively. Most important findings are the commutativity of the TWA and depth-averaging operators, $\widehat{[\psi]} = [\hat{\psi}]$ [see (8)], and thus the independence of the depth-averaged TWA $[\hat{\psi}]$ on the vertical coordinate.

$\widehat{[\psi]}$	$=$	$[\hat{\psi}]$	$\neq$	$[\langle\psi\rangle]$	$\neq$	$\langle[\psi]\rangle$
$\shortparallel$		$\shortparallel$		$\nparallel$		$\shortparallel$
$[\widehat{\psi^\sigma}]$	$=$	$[\hat{\psi}^\sigma]$	$\neq$	$[\langle\psi^\sigma\rangle]$	$=$	$\langle[\psi^\sigma]\rangle$
$\shortparallel$		$\shortparallel$		$\nparallel$		$\shortparallel$
$[\widehat{\psi^z}]$	$=$	$[\hat{\psi}^z]$	$=$	$[\langle\psi^z\rangle]$	$\neq$	$\langle[\psi^z]\rangle$

c. The generalized TWA concept

The TWA operator in (9) is only valid for a nonzero, single-signed Jacobian $\partial z/\partial s$ which requires a strictly monotonic coordinate function $s(z)$, see section 2a. Geometric coordinates (e.g., geopotential and σ coordinates) are strictly monotonic. In contrast, this constraint is not fulfilled by arbitrary isotracer coordinates (e.g., isohaline coordinates), because single tracer values can occur at multiple positions in the water column. To investigate residual dynamics in isohaline coordinates, MacCready (2011) developed the TEF analysis [see also Burchard et al. (2018) and earlier concepts by Walin (1977)]. The fundamental quantity of the TEF analysis is the tidally averaged volume flux per salinity class $-\partial\left\langle\iint_{A\{S^z(x',z')>S\}} u^z(x', z')\, dx'\, dz'\right\rangle/\partial S$. The superscript in S^z is explicitly stated to distinguish the salinity distribution $S^z(x', z')$ at the cross section from the salinity value S of the specific salinity class. Thus, the surface integral only counts those parts of the cross section with salinities higher than S. Following Wolfe (2014), this condition can be reformulated by means of the Heaviside function

$$\mathscr{H}\{x\} = \begin{cases} 0 & \text{for } x \le 0, \\ 1 & \text{for } x > 0. \end{cases} \quad (11)$$

After exchanging the order of differentiation and tidal averaging the tidally averaged volume flux per salinity class can be written as $\langle-\partial Q_>/\partial S\rangle$, with $Q_>(S) = \iint\mathscr{H}\{S^z(x', z') - S\} u^z(x', z')\, dx'\, dz'$ being the volume flux in salinity space above a prescribed salinity level S.

In the following this approach is applied to a generalized vertical coordinate s and the relation to the TWA concept is demonstrated for nonmonotonic coordinate functions $s(z)$. Without loss of generality a single water column is considered for simplicity (see last paragraph in section 2b). In this context the transport $M_>(s)$ above a prescribed coordinate level s and the associated thickness $D_>(s)$ are defined as

$$M_>(s) = \int_{-H}^{\eta} \mathscr{H}\{s^z(z') - s\} u^z(z')\, dz', \quad (12a)$$

$$D_>(s) = \int_{-H}^{\eta} \mathscr{H}\{s^z(z') - s\}\, dz'. \quad (12b)$$

The transport across the whole water column, that is, for $s > -\infty$, reproduces the depth-integrated transport defined in (3): $M_>(-\infty) = M$. In analogy $D_>(-\infty) = D$. In contrast to the Eulerian residual transport velocity $\hat{U}$ in (4), the TWA velocity $\hat{u}$ is defined as the residual transport velocity in an infinitesimal band around a prescribed s level in terms of the differential transport $-\partial M_>/\partial s$ and the differential thickness $-\partial D_>/\partial s$,

$$\hat{u}(s) = \frac{\left\langle-\dfrac{\partial M_>}{\partial s}(s)\right\rangle}{\left\langle-\dfrac{\partial D_>}{\partial s}(s)\right\rangle} = \frac{\left\langle\displaystyle\int_{-H}^{\eta} \delta\{s^z(z') - s\} u^z(z')\, dz'\right\rangle}{\left\langle\displaystyle\int_{-H}^{\eta} \delta\{s^z(z') - s\}\, dz'\right\rangle}, \quad (13)$$

with $\delta\{x\} = d\mathscr{H}\{x\}/dx$ being the Dirac δ distribution. By construction, (13) maps data from z coordinates to s levels and does not require any constraints on the function $s(z)$. For strictly monotonic functions a unique coordinate transformation exists and the integrals in (13) can be transformed by means of $\int_{-H}^{\eta} dz'\delta\{s^z(z') - s\} = \int_{-\infty}^{+\infty} ds'|\partial z/\partial s|\delta\{s' - s\}$. In this case the sampling property of the δ distribution simplifies the differential transport and thickness to $-\partial M_>/\partial s = |\partial z/\partial s|u$ and $-\partial D_>/\partial s = |\partial z/\partial s|$, respectively. Thus, the generalized TWA velocity (13) recovers the original definition $\hat{u} = \langle|\partial z/\partial s|u\rangle/\langle|\partial z/\partial s|\rangle$ based on (9). Although the focus has been on velocity in this section, the definition of the generalized TWA in (13) is of course also valid for any quantity ψ with (9) being the special case for a strictly monotonic vertical coordinate function (Wolfe 2014):

$$\hat{\psi}(s) = \frac{\left\langle\displaystyle\int_{-H}^{\eta} \delta\{s^z(z') - s\}\psi^z(z')\, dz'\right\rangle}{\left\langle\displaystyle\int_{-H}^{\eta} \delta\{s^z(z') - s\}\, dz'\right\rangle}. \quad (14)$$

Appendix B explains the remapping for discrete data, used in section 3c to analyze numerical model results.

3. Examples

a. Analytical tidal estuary flow

For the purpose of demonstrating the different tidal-averaging operators (1) and (9), idealized analytical profiles are constructed for velocity u and suspended

particulate matter (SPM) concentration c over one tidal cycle by temporally concatenating individual steady-state solutions to the one-dimensional set of stationary equations

$$0 = -g\frac{\partial \eta}{\partial x} + (\eta - z)\frac{\partial b}{\partial x} + \frac{\partial}{\partial z}\left(\nu\frac{\partial u}{\partial z}\right), \qquad (15a)$$

$$0 = -\frac{\partial}{\partial z}\left(w_c c - \nu_c\frac{\partial c}{\partial z}\right). \qquad (15b)$$

The simplified set (15a) and (15b) is obtained from the full equations (A2) and (A4) by assuming nonrotating flow in a local pressure gradient–friction balance (Baumert and Radach 1992; Burchard 2009), and horizontal homogeneity, except for a prescribed along-estuary buoyancy gradient $\partial b/\partial x$, which is uniform over depth, and the surface slope $\partial\eta/\partial x$, which formally serves to enforce $[u] = U$ [see Burchard (1999) for details]. Hansen and Rattray (1965) studied a similar form of the momentum equation, but for a fixed local surface elevation $\eta = 0$ and with a constant eddy viscosity ν. Here, more realistic parabolic profiles of eddy viscosity and diffusivity ν_c proportional to the tidally varying bottom friction velocity are considered; see (C2a). The corresponding boundary conditions as well as the analytical solution to (15a) and (15b) for a constant settling velocity $w_c < 0$, derived by Burchard and Hetland (2010) and Burchard et al. (2013), are given in appendix C. In contrast to the original studies dealing with tidally averaged equations, here stationarity and the assumptions mentioned above represent a severe oversimplification of the varying dynamics within a tidal cycle. Nevertheless, for the focus of the present study, the analytical solutions offer a straightforward demonstration of the different averaging techniques.

The individual solutions at different time stages are coupled by a prescribed tidal cycle for the surface elevation η and the depth-averaged velocity U:

$$\eta(t) = \eta_a \cos\left(2\pi\frac{t}{T}\right), \qquad (16a)$$

$$U(t) = \langle U \rangle + U_a \cos\left(2\pi\frac{t}{T} + \phi\right). \qquad (16b)$$

The phase shift of the velocity relative to the surface elevation is denoted by ϕ, where $\phi = 0$ represents a tidal wave with maximum flood during high water, and $\phi = \pi/2$ represents a tidal wave with slack water at high and low water. Depending on the amplitudes η_a and U_a, the residual velocity $\langle U \rangle$ is adjusted to guarantee a prescribed Eulerian residual transport velocity $\hat{U}$ (representing a prescribed river runoff

velocity). The required relation can be obtained by combination of (16a), (16b), and (4):

$$\langle U \rangle = \hat{U} - \frac{U_a \eta_a}{2\langle D \rangle}\cos(\phi). \qquad (17)$$

Analytical velocity profiles have been calculated from (C4a) at 1000 time stages covering one tidal cycle at 1000 equidistant σ and z levels, respectively. Figures 1a–c show results for a tidal wave with $\phi = \pi/4$ at $\langle D \rangle = 10\,\mathrm{m}$ mean water depth, an Eulerian residual transport velocity of $\hat{U} = -0.02\,\mathrm{m\,s^{-1}}$ (negative velocities indicate down-estuary flow), a tidal velocity amplitude of $U_a = 1\,\mathrm{m\,s^{-1}}$, and three tidal elevation amplitudes of $\eta_a = 0\,\mathrm{m}$, $\eta_a = 1\,\mathrm{m}$, and $\eta_a = 5\,\mathrm{m}$. The extreme case of $\eta_a = 5\,\mathrm{m}$ only serves as a formal test of the averaging procedures for large tidal ranges (where the assumption of a linear wave, $\eta_a/H \ll 1$, is not appropriate anymore). The buoyancy gradient and the bottom roughness length were set to $\partial b/\partial x = 1 \times 10^{-5}\,\mathrm{s^{-2}}$ (denser water in down-estuary direction) and $z_0 = 0.01\,\mathrm{m}$, respectively.

For all values of η_a, bidirectional exchange flow occurs during low-current velocities (near slack tide) when the eddy viscosity is small, a process which has been described by several authors (e.g., Stacey et al. 2008). It is also apparent that flood profiles are more uniform than ebb profiles, due to the superposition of classical logarithmic flow profiles with estuarine exchange flow. Residual flow profiles are shown in Figs. 1d–f. For a fixed surface elevation, that is, $\eta_a = 0$, the profiles of the Eulerian residual velocity $\hat{u}^z$, the TWA velocity in σ coordinates $\hat{u}^\sigma$ and the residual velocity $\langle u^\sigma \rangle$ are identical and exhibit residual up-estuary flow near the bottom and down-estuary flow near the surface. However, $\hat{u}^z$ and $\hat{u}^\sigma$ diverge with increasing tidal elevation amplitude. The Eulerian residual velocity shows a residual circulation with up-estuary flow in the range of the oscillating free surface, compensated by stronger down-estuary flow below the low water level and also down-estuary flow near the bottom. In contrast, $\hat{u}^\sigma$ continues to show classical estuarine circulation. The residual velocity $\langle u^\sigma \rangle$ is down estuary and, in contrast to $\hat{u}^z$ and $\hat{u}^\sigma$, does not recover the prescribed Eulerian residual transport velocity when vertically averaged ($[\langle u^\sigma \rangle] = \langle U \rangle \neq \hat{U}$, see section 2b). The extreme case of $\eta_a = 5\,\mathrm{m}$ yields a depth-averaged residual velocity of $[\langle u^\sigma \rangle] = \langle U \rangle = -0.20\,\mathrm{m\,s^{-1}}$, significantly deviating from the Eulerian residual transport velocity $\hat{U} = [\hat{u}^z] = [\hat{u}^\sigma] = -0.02\,\mathrm{m\,s^{-1}}$ (equivalent to the prescribed river runoff velocity) and clearly demonstrating the nonconservativity of $\langle u^\sigma \rangle$.

Analytical SPM profiles for a settling velocity of $w_c = -2 \times 10^{-3}\,\mathrm{m\,s^{-1}}$ have been calculated from (C4b). Figure 2a–c shows the tidally resolved SPM profiles
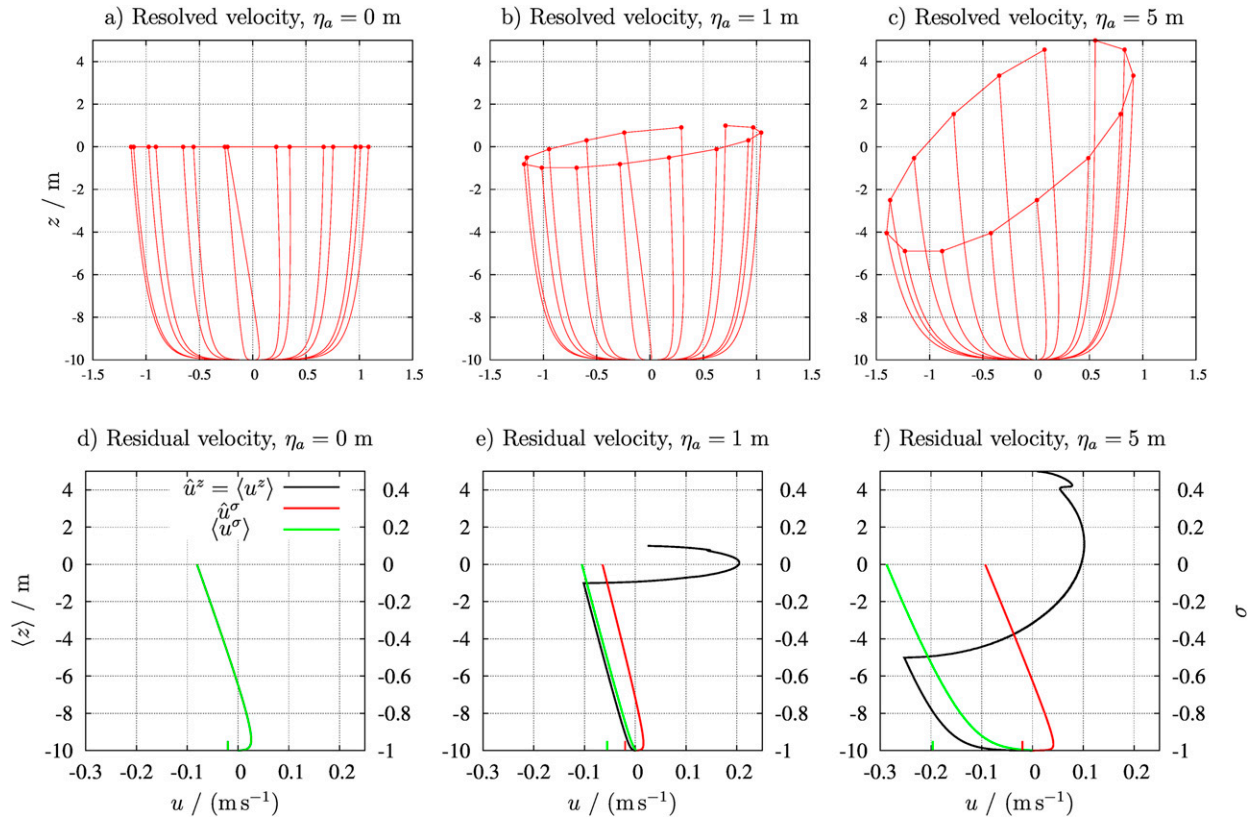
FIG. 1. Velocity profiles computed from the analytical solution for tidal flow with three different tidal elevation amplitudes (section 3a). (a)–(c) Instantaneous velocity profiles u during one tidal cycle. (d)–(f) Residual velocity profiles: $\hat{u}^z = \langle u^z \rangle$ (black), $\hat{u}^\sigma$ (red), $\langle u^\sigma \rangle$ (green). The short marks at the bottom of (d)–(f) mark the respective depth-averaged velocities: $[\hat{u}^z] = [\hat{u}^\sigma] = \hat{U}$ (red; equivalent to the prescribed river runoff velocity), $[\langle u^\sigma \rangle] = \langle U \rangle$ (green). For $\eta_a = 0$ in (d) the profiles of $\hat{u}^z$, $\hat{u}^\sigma$, and $\langle u^\sigma \rangle$ are identical. The kink of $\hat{u}^z$ near the surface in (e) and (f) is caused by the singularity of (C4a) for $u_*^b = 0$ occurring at slack tide. The ordinate axes in (d)–(f) are related by $\langle z \rangle = \sigma H = \langle z(\sigma) \rangle$ to present the residual velocities in σ coordinates also with reference to the mean geopotential position. This choice implies that $\hat{u}^z$ is only presented with reference to the fixed z [and not with reference to $\langle \sigma(z) \rangle$].

associated with the corresponding velocity profiles of Figs. 1a–c. The residual SPM profiles are shown in Figs. 2d–f. As for the velocity, the residual SPM profiles in σ and z coordinates are identical for a fixed surface elevation. In contrast, for tidal waves with oscillating surface elevations the Eulerian SPM concentration $\hat{c}^z$ is smeared out within the tidal range. The profiles of residual SPM concentration in σ coordinates $\hat{c}^\sigma$ are almost identical for different tidal elevation amplitudes, although the instantaneous solutions (C4b) are classical Rouse profiles that depend on the water depth D and the depth-averaged velocity U, which are both time dependent.

The resulting tidally resolved SPM fluxes uc are shown in Figs. 3a–c, with zero values at the surface (due to the Rouse profile) and zero values at the bottom (due to the no-slip condition for velocity). The residual SPM flux profiles in σ and z coordinates (Figs. 3d–f) are identical for a fixed surface elevation. The exchange profile exhibits

up-estuary transport near the bottom and down-estuary transport near the surface, with a small negative depth-averaged TWA flux ($[\widehat{uc}] < 0$). When the tidal range increases, the TWA flux in σ coordinates $\widehat{uc}^\sigma$ still shows this exchange profile, however now with increased amplitude. In contrast, the Eulerian residual SPM flux $\widehat{uc}^z$ shows an exchange profile with up-estuary transport near the surface and down-estuary transport near the bottom.

b. Field data from a tidal channel in the Wadden Sea

In this section in situ observations of along-channel current velocity and SPM concentration in a tidal channel, as presented by Becherer et al. (2016), are analyzed to compare residual quantities in σ coordinates and geopotential coordinates. The data have been observed during 2 days in May 2011 in the southern Wadden Sea of the German Bight, southeastern North Sea. During that period, the landward water was about 4 K warmer
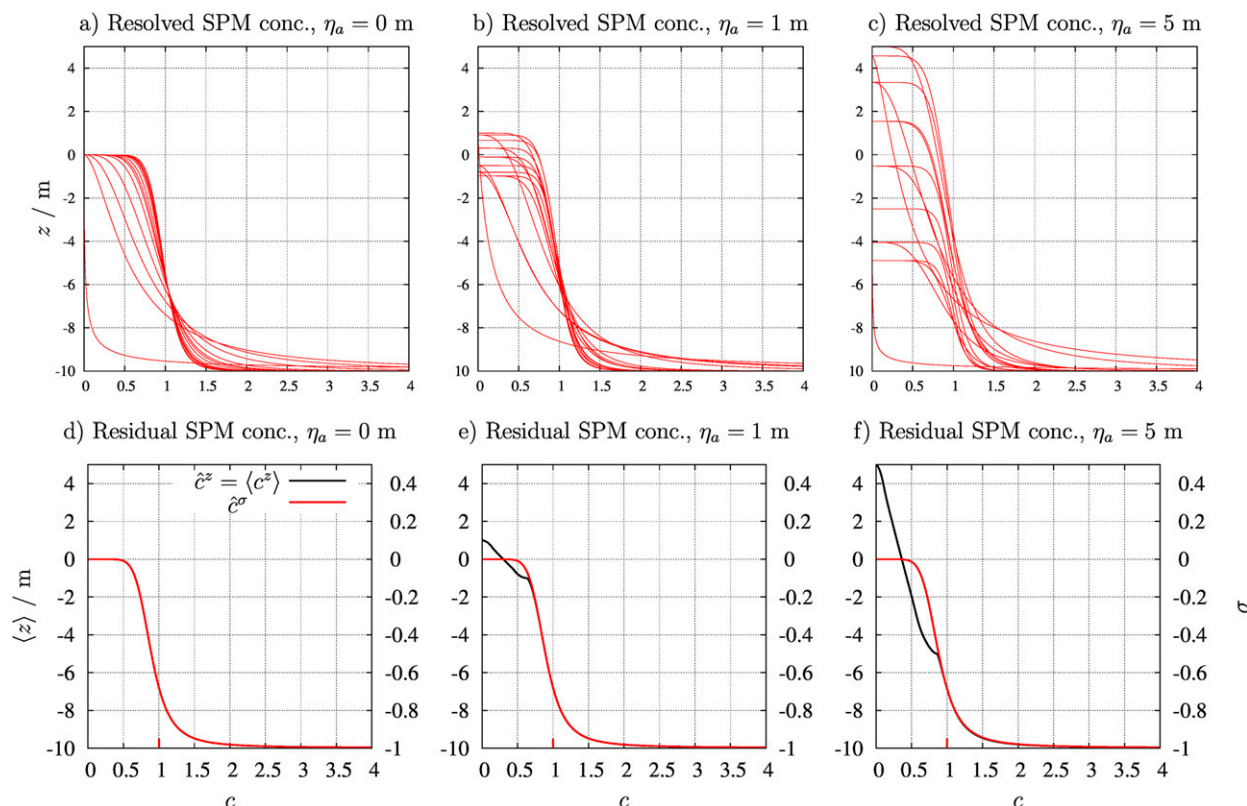
FIG. 2. As in Fig. 1, but for SPM concentration c as presented by Eq. (C4b). For $\eta_a = 0$ in (d) the profiles of $\hat{c}^z$ and $\hat{c}^\sigma$ are identical.

than the seaward water, with only a small salinity difference, such that a classical estuarine density gradient was established. During the campaign, the research vessel was anchored in a tidal channel of about 13 m depth. Velocity data are from a vessel-mounted acoustic Doppler current profiler (ADCP) and SPM data are from a turbidity sensor mounted in a free-falling microstructure profiler operated from the ship. Turbidity data were calibrated against water samples to obtain SPM concentrations. The tidal range was about 2 m during the observation period and due to the swing of the vessel at the anchor with the semidiurnal tidal current, the vertical position of the bottom was variable in time as well. Further details of the campaign and the data analysis are given in Becherer et al. (2015) and Becherer et al. (2016). All data were vertically interpolated to a grid of 20 equidistant σ layers and short data gaps within each layer were filled by temporal along-layer interpolation. To test the averaging procedures for water columns with only partial data coverage, missing data in the vicinity of the bottom and free surface were not filled by extrapolation (see, e.g., Giddings et al. 2014), but by zero values. Consequently, the velocity in the lowermost σ layer above the bottom and the four uppermost σ layers below the surface was set to zero. The same holds for the SPM concentration

in the uppermost σ layer below the surface. Vertical interpolation to 170 equidistant geopotential layers provided the instantaneous profiles for the Eulerian residuals. All residual quantities are obtained as running means over an averaging period of two M_2 cycles. The available measurements do not offer a longer averaging window, usually applied to analyze subtidal residuals.

The along-channel velocity data are presented in Fig. 4. The tidally resolved velocity (Fig. 4a) shows a tidal wave with slack after flood occurring shortly after high water. This includes a long ebb-to-flood transition during low water and a short flood-to-ebb transition during high water. Maximum ebb velocities are higher than maximum flood velocities, partly due to the curvature of the tidal channel leading to a weak ebb dominance at the anchor position (see Becherer et al. 2015). The TWA velocity in σ coordinates $\hat{u}^\sigma$ (Fig. 4b) exhibits a classical estuarine exchange flow due to the horizontal density gradient, overlaid by a subtidal change in the tidal asymmetry. In contrast, the Eulerian residual velocity $\hat{u}^z$ (Fig. 4c) shows relatively strong landward flow within the upper coordinate levels, strong seaward flow very close to the bottom and a slightly seaward-biased exchange flow in between (also see mean residual velocity profiles in Fig. 4d).
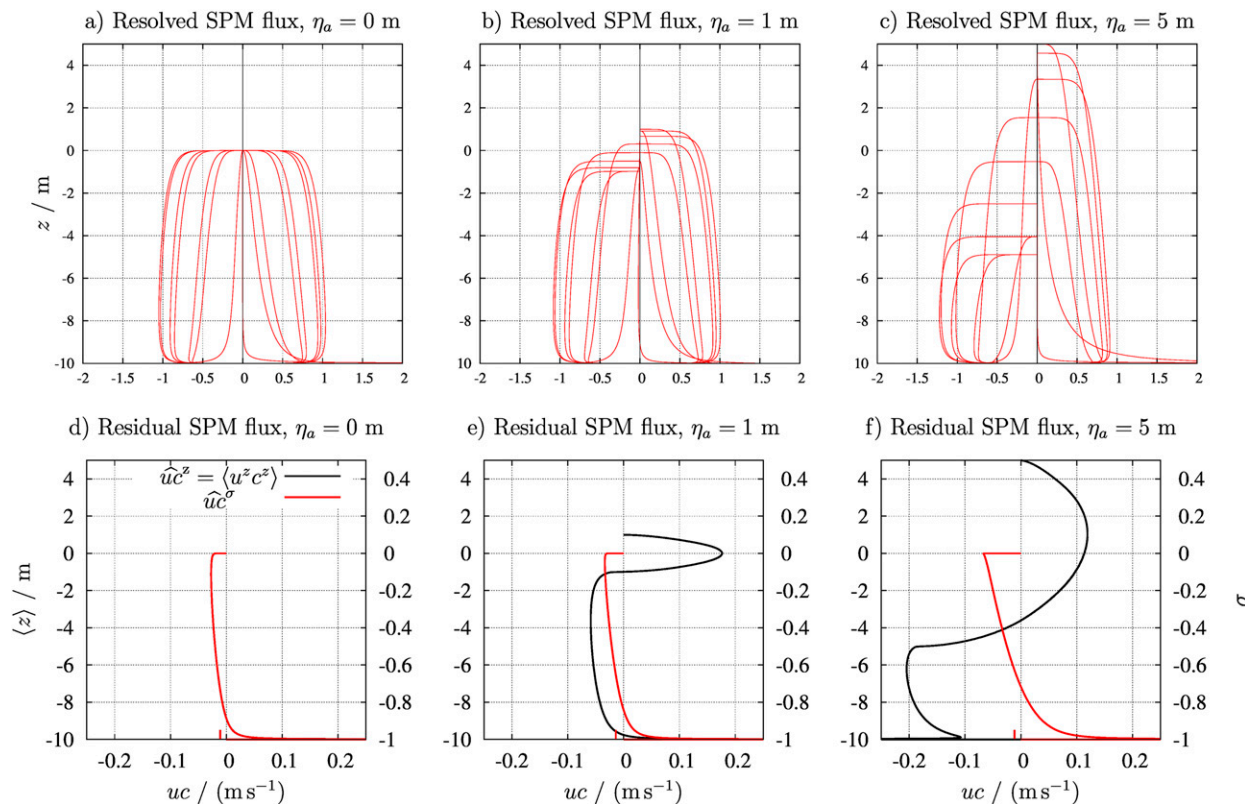
FIG. 3. As in Fig. 1, but for SPM flux uc. For $\eta_a = 0$ in (d) the profiles of $\widehat{uc}^z$ and $\widehat{uc}^\sigma$ are identical.

Sediment concentration (see Fig. 5) is elevated during maximum ebb and flood, with slightly higher ebb values. A local concentration maximum is visible near the surface mainly during ebb and low tide, caused by SPM transport from the adjacent tidal flats (Becherer et al. 2016). The TWA concentration profile in σ coordinates $\hat{c}^\sigma$ is similar to a classical Rouse profile except for the surface values. The Eulerian residual concentrations $\hat{c}^z$ are similar, except for almost zero values toward the surface and very close to the bottom.

SPM flux profiles are presented in Fig. 6. The TWA flux in σ coordinates $\widehat{uc}^\sigma$ is ebb-dominated with seaward transport slightly increasing toward the surface. The Eulerian residual flux profile $\widehat{uc}^z$ is similar, but with landward transport within the uppermost coordinate levels, increased seaward transport below and a strong peak of seaward transport very close to the bottom. Despite the residual landward flow in the lower water column (except for the very near bottom seaward peak in $\hat{u}^z$, see Figs. 4c,d) the corresponding residual SPM fluxes are directed seaward.

The water column is only very weakly stratified during the measurement campaign. Similar to the Eulerian sediment concentration, also $\hat{\rho}^z$ vanishes toward the surface and very close to the bottom. Therefore, in

Figs. 4–6c averaged isopycnals are only shown at depths where density data are available throughout the full averaging period.

c. Numerical model of a two-dimensional tidal estuary

Warner et al. (2005) set up an idealized two-dimensional tidal estuary for numerical model studies. Adopting the slight modifications from Burchard et al. (2019), the present application simulates an estuary of 100 km length, with a water depth that decreases linearly from 15 m at the open ocean boundary to 5 m at the river end. A sinusoidal semidiurnal tide with an elevation amplitude of 0.6 m is prescribed at the ocean side. The vertically integrated freshwater runoff from the river is set to $0.1\,\mathrm{m}^2\,\mathrm{s}^{-1}$ (equivalent to $50\,\mathrm{m}^3\,\mathrm{s}^{-1}$ for an estuary of 500 m width). All water up to 30 km from the ocean boundary is initialized with a salinity of $30\,\mathrm{g\,kg}^{-1}$. The last 20 km closest to the river end are initially covered by freshwater. A linear down-estuary salinity gradient is prescribed over the intermediate portion of the estuary. At the open ocean boundary the initial salinity is held fixed during the course of the simulation. The simulation (for details see Burchard et al. 2019) is carried out with the coastal ocean model GETM (Burchard and Bolding 2002;
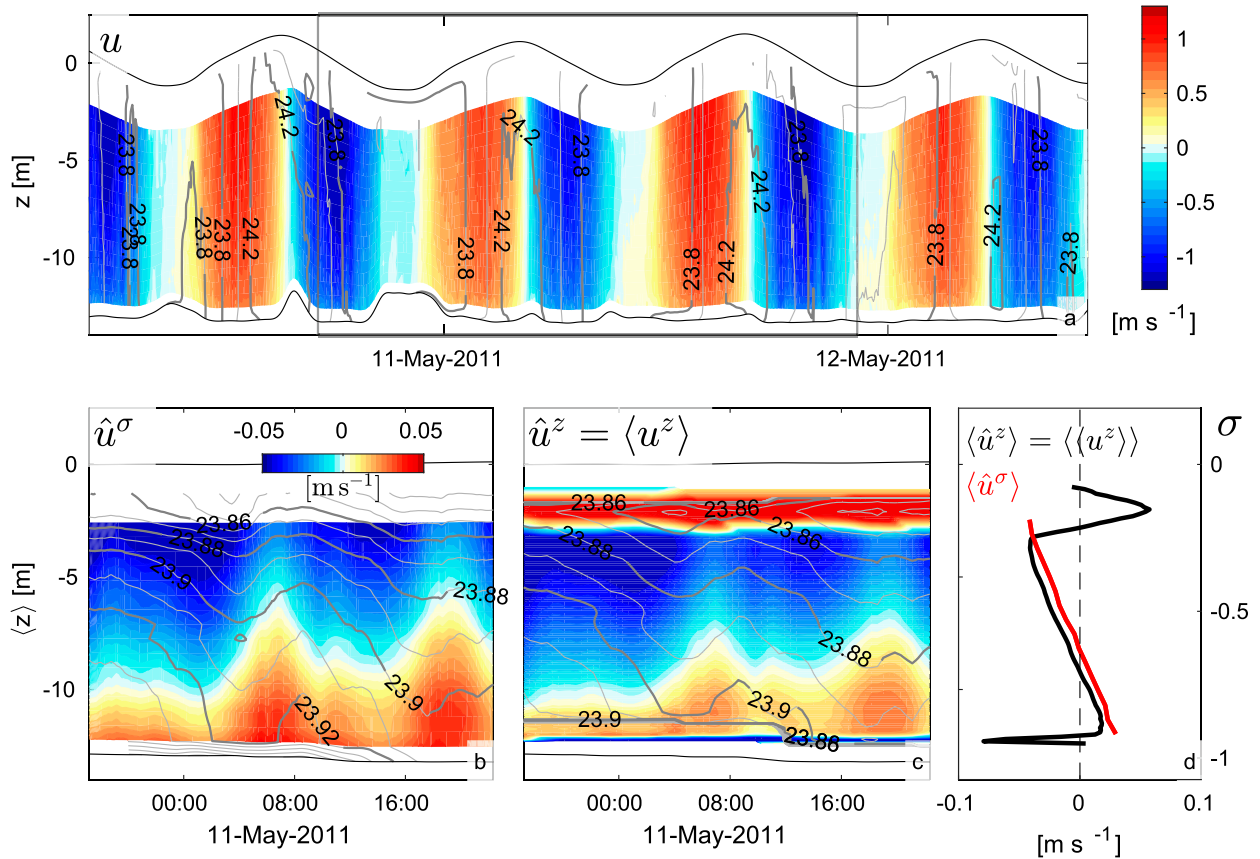
FIG. 4. Along-channel velocity in a tidal channel (section 3b). (a) Observed velocity u. (b),(c) Residual velocities $\hat{u}^\sigma$ and $\hat{u}^z = \langle u^z \rangle$, respectively. (d) Mean residual velocities: $\langle \hat{u}^z \rangle = \langle \langle u^z \rangle \rangle$ (black), $\hat{u}^\sigma$ (red). In (a) the black lines indicate the position of the bottom and the free surface, respectively, and the box marks the time span for which residual velocities are computed. Residual velocities and bottom and free surface positions in (b) and (c) are obtained as running means over an averaging period of two M_2 cycles ($T \approx 24.8$ h). The mean residual quantities in (d) are simple time averages over the time span of available residual data. In (b) $\hat{u}^\sigma$ is presented with reference to the mean geopotential position $\langle z(\sigma) \rangle$. The ordinate axes in (d) are related by $\langle \langle z \rangle \rangle = \langle \langle \eta \rangle \rangle + \sigma \langle \langle D \rangle \rangle = \langle \langle z(\sigma) \rangle \rangle$. This choice implies that $\langle \hat{u}^z \rangle$ is only presented with reference to the fixed z [and not with reference to $\langle \langle \sigma(z) \rangle \rangle$]. Isopycnals are depicted by gray contour lines in (a)–(c). In (c) averaged isopycnals $\hat{\rho}^z$ are only shown at depths where density data are available throughout the full averaging period.

Hofmeister et al. 2010; Klingbeil and Burchard 2013). After a spinup of 100 tidal cycles, an almost periodic state is reached and residual quantities are calculated over the next subsequent 10 tidal cycles. Residuals are obtained in the 40 equidistant σ layers of the model, 134 equidistant z bins ($\Delta z = 0.1$ m) and 70 equidistant salinity bins ($\Delta S = 0.25$ g kg^{-1}). For geopotential and salinity coordinates, the residuals are calculated as described in appendix B. Profiles of residual velocity, salinity and salinity flux at 22.5 km up-estuary from the open-ocean boundary are shown in Fig. 7.

The TWA velocity in σ coordinates $\hat{u}^\sigma$ (Fig. 7a) shows a classical estuarine circulation profile. Except for up-estuary flow in the range of the oscillating free surface and a slightly down-estuary shifted profile, the Eulerian residual velocity $\hat{u}^z$ (Fig. 7a) shows similar exchange flow. The TWA velocity in salinity coordinates

$\hat{u}^S$ (Fig. 7d) is of the same order of magnitude as $\hat{u}^z$ and $\hat{u}^\sigma$. It indicates residual inflow at high salinities and residual outflow at intermediate salinities. The highest residual velocities are associated with outflowing brackish water. In all coordinate systems the velocity profiles yield an Eulerian residual transport velocity of $\hat{U} = [\hat{u}^z] = [\hat{u}^\sigma] = [\hat{u}^S] = -0.008$ m s^{-1}, which is equivalent to an Eulerian residual transport of $\langle M \rangle = -0.1$ m^2 s^{-1} and recovers the prescribed river runoff.

The residual salinity profiles $\hat{S}^\sigma$ and $\hat{S}^z$ (Fig. 7b) differ only slightly and show stable residual stratification. In the range of the oscillating free surface the Eulerian residual salinity $\hat{S}^z$ decreases to zero.

The residual salinity fluxes $\widehat{uS}^\sigma$ and $\widehat{uS}^z$ (Fig. 7c) are similar to the profiles of the residual velocities. In contrast, the residual salinity flux in salinity coordinates $\widehat{uS}^{\bar{S}}$ (Fig. 7f) shows a linear rescaling of the velocity profile $\hat{u}^S$
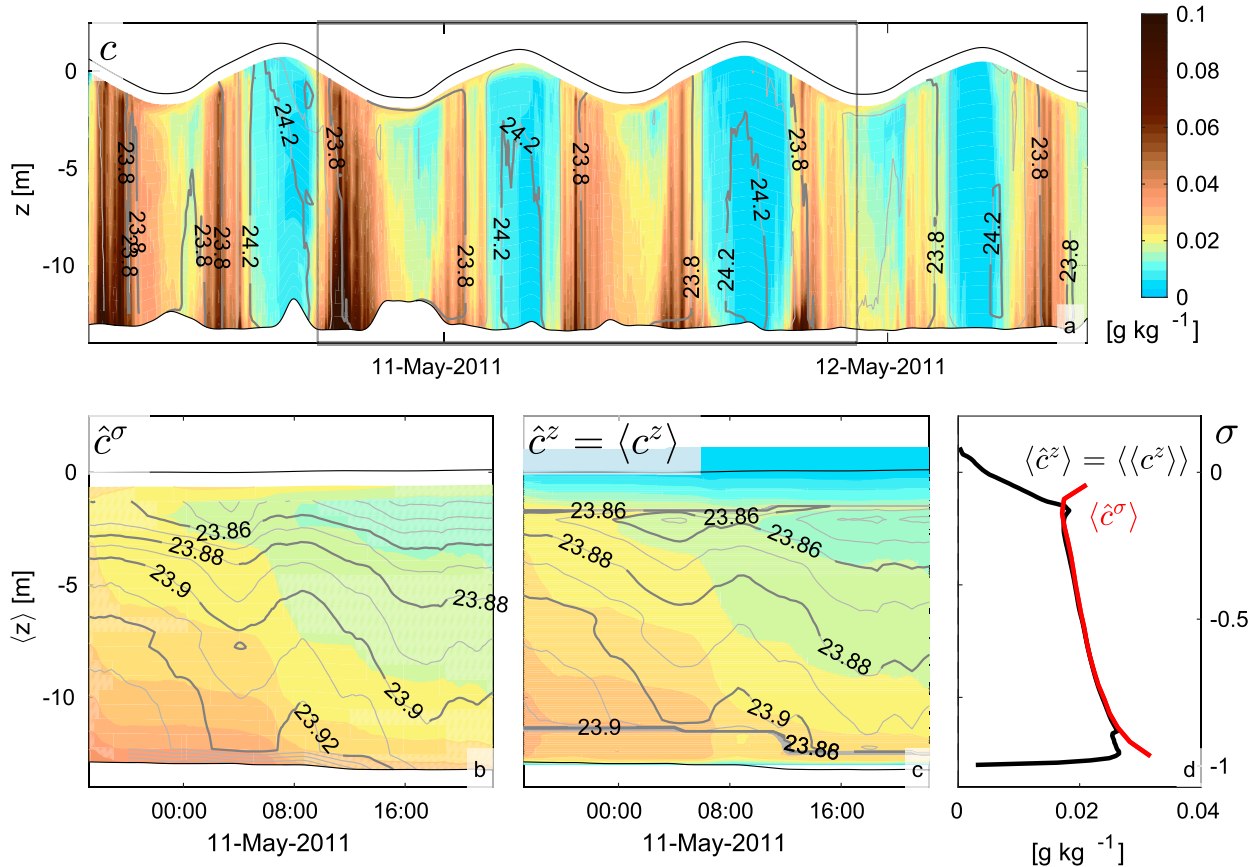
FIG. 5. As in Fig. 4, but for SPM concentration c.

proportional to S, causing a levelled down-estuary residual salinity flux for brackish waters and an amplified up-estuary residual salinity flux at high salinities.

Figure 7e shows the residual differential thickness $\langle -\partial D_>/\partial S\rangle$ of the salinity bins. A nonzero thickness underlines that a vanishing residual flux for a bin is a result of compensating inflows and outflows of identical salinity throughout a tidal cycle. Identical in- and outflowing salinities do not imply no mixing inside the estuary, as the mixing with lower and higher salinities can be balanced. The tiny thickness of low-salinity bins indicates the rather small residual volume and salt outflow associated with the high down-estuary velocity of brackish water.

d. Analysis of results

For all examples, the profiles of the TWA velocity in σ coordinates $\hat{u}^\sigma$ show classical estuarine circulation, also for large tidal ranges. In the analytical test case the Eulerian residual velocity $\hat{u}^z$ is identical to $\hat{u}^\sigma$ for a fixed surface elevation, but shows a transition to stronger inverse-like estuarine circulation for an increasing tidal range (Figs. 1d–f). The latter is a consequence of an increased down-estuary velocity $\langle U\rangle$ according to (17), and a peak of residual up-estuary flow in the range of the oscillating free surface because of no compensating down-estuary velocities in z levels above the low water level (masked with zero velocity when void of water during ebb). This peak of residual up-estuary velocity in the upper coordinate levels is also present in $\hat{u}^z$ from the field data (Figs. 4c,d) and the model estuary (Fig. 7a). However, these examples do not show inverse-like estuarine circulation. Below the peak in the uppermost coordinate levels the profile of $\hat{u}^z$ is only slightly shifted down-estuary with respect to $\hat{u}^\sigma$. These similarities in residual velocity profiles are related to the nearly vertically uniform instantaneous velocity profiles,[1] contrary to the dominantly logarithmic profiles of the analytical case. The TWA velocity in isohaline coordinates $\hat{u}^S$ from the model estuary (Fig. 7d) provides another view on estuarine circulation, showing residual inflow at high

---

[1] A relation between $\hat{u}^\sigma$ and $\hat{u}^z$ can be derived based on Taylor series expansion $u^\sigma(\sigma) \approx u^z(\sigma\langle D\rangle) + (1+\sigma)\eta\partial u^z/\partial z$. See (A2) in Cheng et al. (2013) for the relation between $\langle u^\sigma\rangle$ and $\hat{u}^z$.
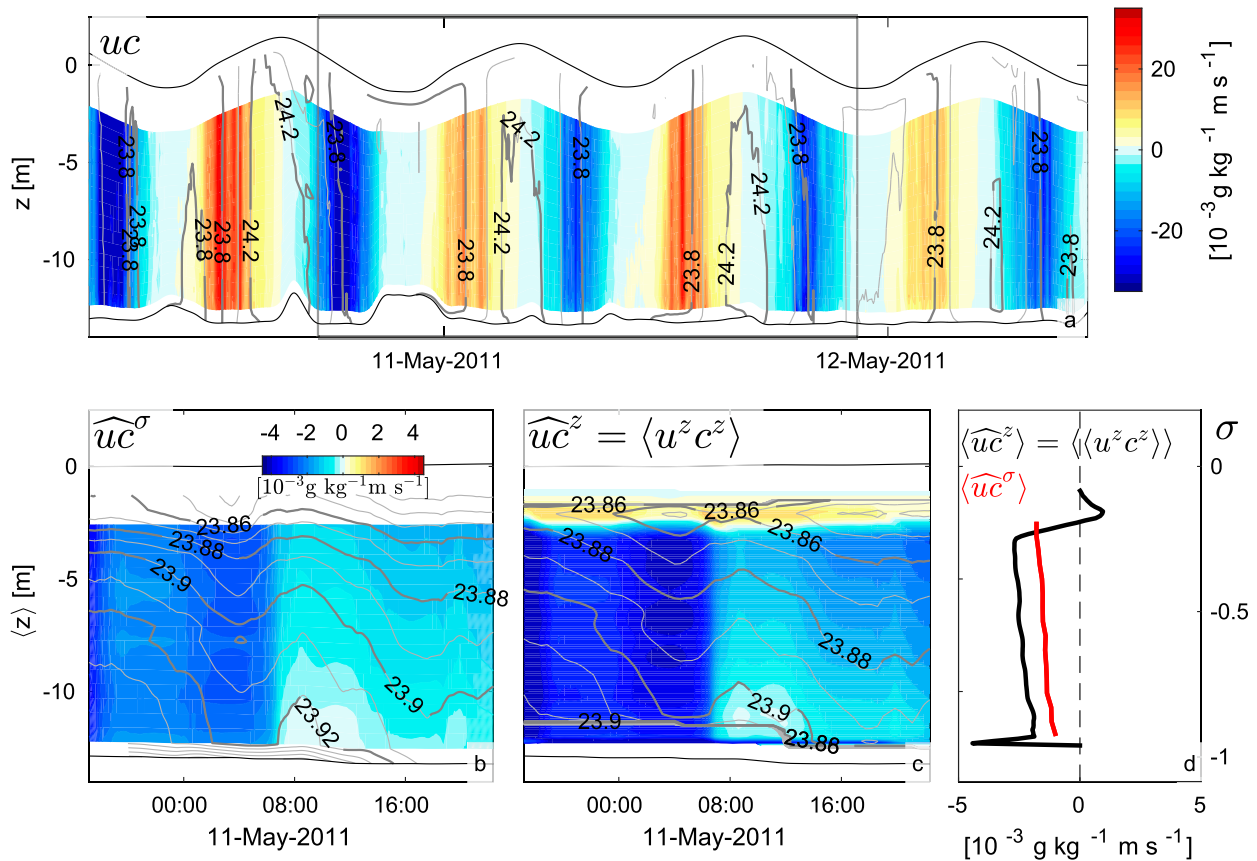
FIG. 6. As in Fig. 4, but for SPM flux uc.

salinities and residual outflow at intermediate and low salinities.

Although caused by the same mechanism during averaging, it is important to classify the described peaks in $\hat{u}^z$ differently. For the analytical test case and the model estuary the high residual up-estuary velocity in the range of the oscillating free surface is caused by the masking of data *outside* the water column with zeros. This masking is valid and consistent with conservative averaging (see section 2b). In contrast, the filling of missing data *inside* the water column with zeros, as done for the Eulerian averaging of the field data (see section 3b), is arbitrary. In this case the resulting peaks are purely mathematical artifacts and do not represent real physical features. Therefore, the upper coordinate levels (landward peak due to missing data during ebb) and the lowermost coordinate levels (seaward peak due to missing data during flood because of a slight drift of the anchored vessel into the shallower parts during flood; see Figs. 4c,d) from the field data should be excluded from the analysis.

These artifacts in the upper and lowermost coordinate levels are also present in $\widehat{uc}^z$ of the field data (Figs. 6c,d). In contrast to the velocity and the SPM flux, field data

for SPM are available for almost the whole water column (Fig. 5). Therefore, the vanishing Eulerian residual concentration $\hat{c}^z$ in the vicinity of the surface (similar to the analytical test case) mainly results from the valid masking above the free surface and should not be classified as artifact. The masking with zero values below the moving bottom causes vanishing $\hat{c}^z$ also close to the bottom. Away from the boundaries, $\hat{c}^z$ and the TWA concentration in σ coordinates $\hat{c}^\sigma$ are almost identical and similar to a classical Rouse profile. It is obvious, that the valid masking of data outside the water column is not only an issue for geopotential coordinates, but for all vertical coordinates that are not boundary-following. For example, the peak of high residual down-estuary velocity for brackish salinities in the model estuary is due to no compensating up-estuary flow of the same salinities during flood (caused by strain-induced periodic stratification; see Simpson et al. 1990).

4. Discussion

It was demonstrated that TWA in σ coordinates provides a simple (no masking of data outside the water
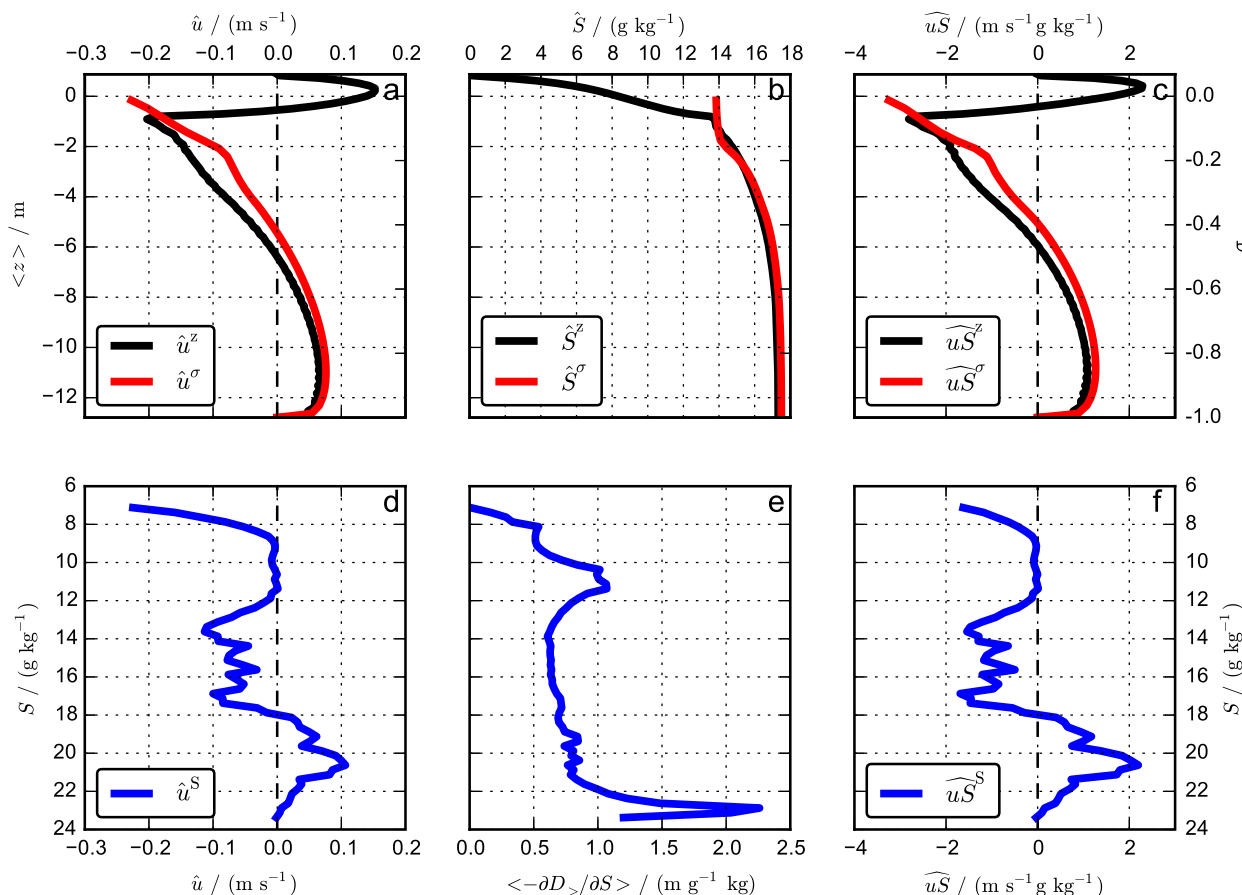
FIG. 7. Residual quantities at 22.5 km up-estuary from the open-ocean boundary in a two-dimensional tidal estuary (section 3c). (a)–(c) Residual velocity, salinity, and salinity flux, respectively, in z (black) and σ coordinates (red). (d)–(f) Residual velocity, differential thickness, and salinity flux, respectively in salinity space.

column is necessary) and conservative framework for calculating residual quantities in tidal estuaries (also see Giddings et al. 2014). The averaging can be applied to a time-varying water depth and is robust also for large tidal ranges (Kjerfve 1975). Averaging in geopotential coordinates is also conservative and the interpretation of the resulting Eulerian residuals is very intuitive (see below). TWA in isohaline coordinates conservatively averages over water masses with identical salinities and offers the analysis of residual dynamics with respect to salinity classes (MacCready 2011).

The vertical profiles of residual quantities obtained in different coordinate systems show different vertical distributions of the residual quantity. These different views, extracted from the same original dataset, provide complementary information about the residual dynamics and are all equally valid. Therefore, the classical results for estuarine circulation [as proposed by Hansen and Rattray (1965)] reproduced by TWA in σ coordinates are as correct as the sometimes

inverse-like estuarine circulation obtained from Eulerian averaging.

The difficulty is in the correct interpretation of these different results. Unweighted tidal averages represent the residual that a fictitious observer would measure by vertically following a specific coordinate line. The relevance of these residuals can be debated. As a special case the Eulerian average simply represents the residual that would be obtained from data measured by a sensor that is mounted at a fixed geopotential position. The interpretation is less intuitive for other coordinate systems, because the resulting residuals are obtained following a varying position and can be referenced only to a mean position (e.g., for graphical presentation). The focus on the mean position can be prone to misinterpretation, as it distracts from the correct interpretation in the transformed space of the applied coordinate system (e.g., the correct interpretation of residuals in isohaline coordinates with respect to salinity classes). Second, the mean position can be misleading, especially in the case

of nonmonotonic coordinate functions $s(z)$, which cause a folding of nonadjacent parts of the water column where the same value of s occurs [see section 2c and Wolfe (2014)]. Another source of misinterpretation is the confusion with Lagrangian residuals. The TWA velocity in σ coordinates shows classical estuarine circulation, but the residuals obtained from TWA in σ coordinates must not be interpreted as Lagrangian residuals. Although the TWA velocity in σ coordinates includes the so-called wave-transport portion of the Stokes drift [e.g., Giddings et al. 2014, their section 3a(3)], it does not represent the residual velocity of particles, but the residual transport velocity through the interface of a (wave-)distorted infinitesimal σ layer. Lagrangian residuals cannot be accurately obtained in a horizontally Eulerian framework (Longuet-Higgins 1969; Zimmerman 1979).

Another word of caution is necessary in the context of the commonly expected similarity of residual quantities for converging coordinate systems. For example, in the ultimate limit of a vanishing tidal range to depth ratio, that is, $\eta/D = 0$, the residual quantities in σ coordinates are identical to the ones in geopotential coordinates. However, the vertical profiles of residual quantities can still diverge significantly for small ratios. Therefore, it is essential to stick to the precise distinction, accurate calculation and correct interpretation of residual quantities in different coordinate systems.

It becomes clear that residual quantities are only meaningful as long as they are linked to the information on how they were obtained. Since a unique nomenclature (considering, e.g., the various options of vertical coordinate systems) is rather impractical, the present paper focused on a clear and consistent operator notation with a superscript indicating the vertical coordinate, which was held fixed during the averaging process. In all coordinate systems care has to be taken to exclude coordinate levels with missing data inside the water column from the analysis of residual dynamics.

5. Conclusions

This paper links and unifies concepts from different disciplines of oceanography. Thickness-weighted averaging (TWA), originally developed for ocean eddy closures in isopycnal coordinates, is presented in a generalized vertical coordinate and applied in the context of tidal averaging. In contrast to an unweighted temporal low-pass filter, TWA is a conservative operator by definition. Furthermore, TWA commutates with depth-averaging. This commutativity can be exploited in analytical studies and also renders depth-averaged TWA quantities to be invariant to the vertical coordinate system. The choice of a vertical coordinate system depends on the specific

purpose of investigation. The original instantaneous data can be remapped between different coordinate systems. Vertical profiles of residual quantities depend on the vertical coordinate that is held fixed during the averaging process. In particular, there is no unique vertical distribution of the Eulerian residual transport $\langle M \rangle$ due to the sensitivity of the TWA velocity $\hat{u}$ to the chosen vertical coordinate system. Ultimately, the correct interpretation of residual quantities requires a thorough understanding of the averaging in a specific coordinate system. In many numerical coastal ocean models the use of sophisticated arbitrary Lagrangian–Eulerian vertical meshes [see review in Klingbeil et al. (2018)] complicates the correct interpretation of time-averaged model output.

APPENDIX A

Governing Equations

Under the hydrostatic and Boussinesq approximation the conservation of mass and the balance of momentum yield the governing equations for the Cartesian velocity components (u, v, w) and an arbitrary tracer c:

$$\left(\frac{\partial u}{\partial x}\right)_z + \left(\frac{\partial v}{\partial y}\right)_z + \frac{\partial w}{\partial z} = 0, \tag{A1}$$

$$\left(\frac{\partial u}{\partial t}\right)_z + \left(\frac{\partial(uu)}{\partial x}\right)_z + \left(\frac{\partial(vu)}{\partial y}\right)_z + \frac{\partial(wu)}{\partial z}$$
$$= +fv - g\frac{\partial\eta}{\partial x} + \left(\frac{\partial}{\partial x}\right)_z \int_z^\eta b\,dz' - \frac{\partial\tau_u}{\partial z}, \tag{A2}$$

$$\left(\frac{\partial v}{\partial t}\right)_z + \left(\frac{\partial(uv)}{\partial x}\right)_z + \left(\frac{\partial(vv)}{\partial y}\right)_z + \frac{\partial(wv)}{\partial z}$$
$$= -fu - g\frac{\partial\eta}{\partial y} + \left(\frac{\partial}{\partial y}\right)_z \int_z^\eta b\,dz' - \frac{\partial\tau_v}{\partial z}, \tag{A3}$$

$$\left(\frac{\partial c}{\partial t}\right)_z + \left(\frac{\partial(uc)}{\partial x}\right)_z + \left(\frac{\partial(vc)}{\partial y}\right)_z + \frac{\partial(wc)}{\partial z}$$

$$= -\frac{\partial}{\partial z}(w_c c + \tau_c). \tag{A4}$$

The subscript z around partial derivatives in (A1)–(A4) denotes the fixed geopotential vertical coordinate during differentiation. For simplicity, atmospheric pressure gradients and horizontal turbulent fluxes are neglected. Vertical turbulent fluxes are denoted by τ. The parameters f and g are the Coriolis parameter and the gravitational acceleration, respectively. Buoyancy b incorporates density effects. Settling of the tracer, for example, SPM, can be prescribed by a negative velocity w_c.

For the following it is sufficient to consider the prototype form of (A1)–(A4),

$$\left(\frac{\partial \varphi}{\partial t}\right)_z + \left(\frac{\partial(u\varphi)}{\partial x}\right)_z + \left(\frac{\partial(v\varphi)}{\partial y}\right)_z + \frac{\partial(w\varphi)}{\partial z} = R_\varphi, \tag{A5}$$

where R_φ represents the corresponding terms on the right hand sides of (A1)–(A4). After transformation to the generalized vertical coordinate s (see section 2a), (A5) reads

$$\left(\frac{\partial\left(\frac{\partial z}{\partial s}\varphi\right)}{\partial t}\right)_s + \left(\frac{\partial\left(\frac{\partial z}{\partial s}u\varphi\right)}{\partial x}\right)_s + \left(\frac{\partial\left(\frac{\partial z}{\partial s}v\varphi\right)}{\partial y}\right)_s$$

$$+ \frac{\partial\left(\frac{\partial z}{\partial s}\dot{s}\varphi\right)}{\partial s} = \frac{\partial z}{\partial s}R_\varphi, \tag{A6}$$

with the dia-surface velocity component

$$\frac{\partial z}{\partial s}\dot{s} = w - \left(\frac{\partial z}{\partial t}\right)_s - u\left(\frac{\partial z}{\partial x}\right)_s - v\left(\frac{\partial z}{\partial y}\right)_s. \tag{A7}$$

Application of a linear temporal low-pass filter that commutates with spatiotemporal derivatives, for example of (1), yields

$$\left(\frac{\partial\left\langle\frac{\partial z}{\partial s}\varphi\right\rangle}{\partial t}\right)_s + \left(\frac{\partial\left\langle\frac{\partial z}{\partial s}u\varphi\right\rangle}{\partial x}\right)_s + \left(\frac{\partial\left\langle\frac{\partial z}{\partial s}v\varphi\right\rangle}{\partial y}\right)_s$$

$$+ \frac{\partial\left\langle\frac{\partial z}{\partial s}\dot{s}\varphi\right\rangle}{\partial s} = \left\langle\frac{\partial z}{\partial s}R_\varphi\right\rangle. \tag{A8}$$

The commutativity of the filter with temporal derivatives is valid by assuming a spectral gap between the tidal and subtidal motions, such that for a suitable tidal-averaging period the filtered tendency term in (A6) can be approximated by $\langle(\partial(\partial z/\partial s\,\varphi)/\partial t)_s\rangle \approx (\partial\langle\partial z/\partial s\,\varphi\rangle/\partial t)_s$.

Rewriting in terms of thickness-weighted averages offers to separate the residual differential thickness $\langle|\partial z/\partial s|\rangle$ from the correlators in (A8) without the introduction of additional covariance terms:

$$\left(\frac{\partial\left(\left\langle\left|\frac{\partial z}{\partial s}\right|\right\rangle\hat{\varphi}\right)}{\partial t}\right)_s + \left(\frac{\partial\left(\left\langle\left|\frac{\partial z}{\partial s}\right|\right\rangle\widehat{u\varphi}\right)}{\partial x}\right)_s$$

$$+ \left(\frac{\partial\left(\left\langle\left|\frac{\partial z}{\partial s}\right|\right\rangle\widehat{v\varphi}\right)}{\partial y}\right)_s + \frac{\partial\left(\left\langle\left|\frac{\partial z}{\partial s}\right|\right\rangle\widehat{\dot{s}\varphi}\right)}{\partial s} = \left\langle\left|\frac{\partial z}{\partial s}\right|\right\rangle\hat{R}_\varphi. \tag{A9}$$

Vertical integration of (A6) under consideration of the kinematic boundary conditions

$$\frac{\partial z}{\partial s}\left(\dot{s} - \frac{\partial s_s}{\partial t} - u\frac{\partial s_s}{\partial x} - v\frac{\partial s_s}{\partial y}\right) = E - P$$

$$\text{at} \quad s = s_s(x, y, t) = s(x, y, z = \eta, t), \tag{A10a}$$

$$\frac{\partial z}{\partial s}\left(\dot{s} - \frac{\partial s_b}{\partial t} - u\frac{\partial s_b}{\partial x} - v\frac{\partial s_b}{\partial y}\right) = 0$$

$$\text{at} \quad s = s_b(x, y, t) = s(x, y, z = -H, t), \tag{A10b}$$

and subsequent tidal averaging yields the prognostic equation for the residual content of φ in the water column

$$\frac{\partial\left(\langle D\rangle\overline{[\varphi]}\right)}{\partial t} + \frac{\partial\left(\langle D\rangle\overline{[u\varphi]}\right)}{\partial x} + \frac{\partial\left(\langle D\rangle\overline{[v\varphi]}\right)}{\partial y} + \langle\varphi_s(E - P)\rangle$$

$$= \langle D\rangle\overline{[R_\varphi]}, \tag{A11}$$

with $\varphi_s(E - P)$ being the surface flux of φ associated with the evaporation rate E and the precipitation rate P. The commutativity relation (8) offers to replace the residual depth-averaged quantities in (A11) by the corresponding depth-averaged TWA quantities and illustrates again the conservative nature of the TWA quantities $\hat{\varphi}$, $\widehat{u\varphi}$, $\widehat{v\varphi}$, and $\hat{R}_\varphi$ in (A9).

For completeness it should be mentioned, that the methods presented in this paper only adopted the first step of the TWA machinery developed for isopycnal coordinates. The full art of TWA in isopycnal coordinates (de Szoeke and Bennet 1993; Young 2012) is exploited by further separation of the TWA fluxes in (A9) for example[2] $\widehat{u\varphi} = \hat{u}\hat{\varphi} + \overline{(u - \hat{u})(\varphi - \hat{\varphi})} = \hat{u}\hat{\varphi} + \widehat{u''\varphi''}$, yielding

---

[2] The assumption of $\langle\langle\psi\rangle\rangle = \langle\psi\rangle$ implies $\langle\langle\psi\rangle\rangle = \langle\psi\rangle = \widehat{\langle\psi\rangle}$ and $\widehat{\hat{\psi}} = \hat{\psi} = \langle\hat{\psi}\rangle$.

$$\left(\frac{\partial\left(\left\langle\left|\frac{\partial z}{\partial s}\right|\right\rangle\hat{\varphi}\right)}{\partial t}\right)_s + \left(\frac{\partial\left(\left\langle\left|\frac{\partial z}{\partial s}\right|\right\rangle\hat{u}\hat{\varphi}\right)}{\partial x}\right)_s + \left(\frac{\partial\left(\left\langle\left|\frac{\partial z}{\partial s}\right|\right\rangle\hat{v}\hat{\varphi}\right)}{\partial y}\right)_s + \frac{\partial\left(\left\langle\left|\frac{\partial z}{\partial s}\right|\right\rangle\hat{s}\hat{\varphi}\right)}{\partial s} = \left\langle\left|\frac{\partial z}{\partial s}\right|\right\rangle\hat{R}_\varphi - \left\langle\left|\frac{\partial z}{\partial s}\right|\right\rangle\nabla\cdot\mathbf{J}_\varphi,$$

$$(A12)$$

$$\text{with}\qquad \nabla\cdot\mathbf{J}_\varphi = \left\langle\left|\frac{\partial z}{\partial s}\right|\right\rangle^{-1}\left(\left(\frac{\partial\left(\left\langle\left|\frac{\partial z}{\partial s}\right|\right\rangle\widehat{u''\varphi''}\right)}{\partial x}\right)_s + \left(\frac{\partial\left(\left\langle\left|\frac{\partial z}{\partial s}\right|\right\rangle\widehat{v''\varphi''}\right)}{\partial y}\right)_s + \frac{\partial\left(\left\langle\left|\frac{\partial z}{\partial s}\right|\right\rangle\widehat{s''\varphi''}\right)}{\partial s}\right).$$

Subsequent transformation to mean geopotential coordinates $\langle z\rangle(s) = \langle z(s)\rangle$ finally results in

$$\left(\frac{\partial\hat{\varphi}}{\partial t}\right)_{\langle z\rangle} + \left(\frac{\partial(\hat{u}\hat{\varphi})}{\partial x}\right)_{\langle z\rangle} + \left(\frac{\partial(\hat{v}\hat{\varphi})}{\partial y}\right)_{\langle z\rangle} + \frac{\partial(w^{\#}\hat{\varphi})}{\partial\langle z\rangle}$$
$$= \hat{R}_\varphi - \nabla\cdot\mathbf{J}_\varphi, \qquad (A13)$$

with $w^{\#} = \left(\frac{\partial\langle z\rangle}{\partial t}\right)_s + \hat{u}\left(\frac{\partial\langle z\rangle}{\partial x}\right)_s + \hat{v}\left(\frac{\partial\langle z\rangle}{\partial y}\right)_s + \hat{s}\left\langle\frac{\partial\langle z\rangle}{\partial s}\right\rangle \neq \hat{w}$.
In the context of ocean eddies, it is the parameterization of the unresolved eddy-induced flux $\mathbf{J}_\varphi$, that is physically most justified in isopycnal coordinates ($s = \rho$). For non-Boussinesq equations the derivations are similar, with density being included in the weighted average (Greatbatch and McDougall 2003).

APPENDIX B

TWA with Discrete Data

Here, the remapping (14) is outlined for discrete data ψ_k^n given at the centers of k_{max} vertical intervals with layer heights Δz_k^n. The indices k and n denote the layer and the time stage, respectively. Based on the corresponding value of the generalized vertical coordinate s_k^n the data should be remapped into l_{max} prescribed bins $]s_{(l-1/2)}, s_{(l+1/2)}]$. For clarity, the procedure is explained first again for velocity. The discrete analogs of (12a) and (12b) are

$$M_{>,(l+1/2)}^n = \sum_{\substack{k=1\\ \{s_k^n > s_{(l+1/2)}\}}}^{k_{max}} \Delta z_k^n u_k^n, \qquad (B1a)$$

$$D_{>,(l+1/2)}^n = \sum_{\substack{k=1\\ \{s_k^n > s_{(l+1/2)}\}}}^{k_{max}} \Delta z_k^n. \qquad (B1b)$$

The transport in one bin and the associated thickness can be defined as

$$M_{(l)}^n = M_{>,(l-1/2)}^n - M_{>,(l+1/2)}^n = \sum_{\substack{k=1\\ \{s_{(l-1/2)} < s_k^n \le s_{(l+1/2)}\}}}^{k_{max}} \Delta z_k^n u_k^n, \qquad (B2a)$$

$$D_{(l)}^n = D_{>,(l-1/2)}^n - D_{>,(l+1/2)}^n = \sum_{\substack{k=1\\ \{s_{(l-1/2)} < s_k^n \le s_{(l+1/2)}\}}}^{k_{max}} \Delta z_k^n. \qquad (B2b)$$

Thus, with the temporal average for discrete data $\langle\psi_{(l)}\rangle$ defined in Table 1, the TWA velocity (13) in one bin is given by

$$\hat{u}_{(l)} = \frac{\langle M_{(l)}\rangle}{\langle D_{(l)}\rangle}. \qquad (B3)$$

The general definition (14) can be discretized as (also see Table 1)

$$\hat{\psi}_{(l)} = \frac{\langle D_{(l)}\psi_{(l)}\rangle}{\langle D_{(l)}\rangle} \qquad (B4)$$

with $D_{(l)}^n$ defined in (B2b) and

$$\psi_{(l)}^n = \frac{1}{D_{(l)}^n}\sum_{\substack{k=1\\ \{s_{(l-1/2)} < s_k^n \le s_{(l+1/2)}\}}}^{k_{max}} \Delta z_k^n \psi_k^n. \qquad (B5)$$

In case of a known strictly monotonic coordinate function $s(z)$ the inverse function $z(s)$ exists and the thickness of a bin should not be calculated according to (B2b) but correctly as

$$D_{(l)}^n = |z^n(s_{(l+1/2)}) - z^n(s_{(l-1/2)})| = |z_{(l+1/2)}^n - z_{(l-1/2)}^n|. \qquad (B6)$$

Furthermore, instead of assigning the content of ψ_k^n from the vertical interval $[z_{k-1/2}^n, z_{k+1/2}^n]$ to a single bin according to (B5), it can be more accurately distributed over several bins according to

$$\psi_{(l)}^n = \frac{1}{D_{(l)}^n} \sum_{k=1}^{k_{\max}} \Delta z_{k,(l)}^n \psi_k^n, \qquad (B7)$$

with

$$\Delta z_{k,(l)}^n = \max\{0, \min\{z_{k+1/2}, z_{(l\pm1/2)}\} - \max\{z_{k-1/2}, z_{(l\mp1/2)}\}\} \quad \text{for} \quad \frac{\partial z}{\partial s} \gtrless 0. \qquad (B8)$$

These consistent modifications guarantee the convergence of (B4) to (9).

If the averaging is carried out directly in the provided vertical intervals each interval represents one bin with $D_{(l)}^n = \Delta z_l^n$ and $\psi_{(l)}^n = \psi_l^n$ and thus $\hat{\psi}_{(l)} = \langle \Delta z_l \psi_l \rangle / \langle \Delta z_l \rangle \equiv \hat{\psi}_l$.

APPENDIX C

Analytical Steady-State Solution

Here, the analytical solution to the set (15a) and (15b) for parabolic eddy viscosity and diffusivity profiles is given. The derivation was originally presented by Burchard and Hetland (2010) and Burchard et al. (2013) for tidally averaged equations, but is also valid for the instantaneous quantities. In σ coordinates (15a) and (15b) read

$$0 = -g\frac{\partial\eta}{\partial x} - \sigma D\frac{\partial b}{\partial x} + D^{-1}\frac{\partial}{\partial\sigma}\left(\nu D^{-1}\frac{\partial u}{\partial\sigma}\right), \quad (C1a)$$

$$0 = -D^{-1}\frac{\partial}{\partial\sigma}\left(w_c c - \nu_c D^{-1}\frac{\partial c}{\partial\sigma}\right), \qquad (C1b)$$

with $\partial\eta/\partial x$ being adjusted in such a way to guarantee $[u] = U$ [see Burchard (1999) for details].

Parabolic eddy viscosity and diffusivity profiles

$$\nu(\sigma) = -\kappa|u_*^b|\sigma((\sigma+1)D + z_0), \qquad (C2a)$$

$$\nu_c(\sigma) = \nu(\sigma)/(1 + z_0/D), \qquad (C2b)$$

with the bed roughness length z_0, the bottom friction velocity $u_*^b = \kappa U/\Gamma$, the van Karman constant $\kappa = 0.4$, and the integration constant

$$\Gamma = \int_{-1}^{0} \ln\left(\frac{(\sigma+1)D + z_0}{z_0}\right) d\sigma = \frac{D+z_0}{D}\ln\left(\frac{D+z_0}{z_0}\right) - 1, \qquad (C3)$$

comply with surface boundary conditions $(\nu\partial u/\partial z)_{\sigma=0} = 0$ and $(\nu_c\partial c/\partial z)_{\sigma=0} = 0$. Additional bottom boundary conditions for no-slip $u(\sigma = -1) = 0$ and no-flux $(w_c c - \nu_c \partial c/\partial z)_{\sigma=-1} = 0$ yield the analytical solution,

$$u(\sigma) = \frac{\frac{\partial b}{\partial x}D^2}{2\kappa|u_*^b|}\left(\frac{1}{2\Gamma}\ln\left(\frac{(\sigma+1)D + z_0}{z_0}\right) - (\sigma+1)\right)$$
$$+ \frac{1}{\Gamma}\ln\left(\frac{(\sigma+1)D + z_0}{z_0}\right)U, \qquad (C4a)$$

$$c(\sigma) = c_b\left(\frac{-\sigma z_0}{(\sigma+1)D + z_0}\right)^{\text{Ro}}, \qquad (C4b)$$

with the bottom SPM concentration c_b and the Rouse number $\text{Ro} = -w_c/(\kappa|u_*^b|)$. The bottom concentration c_b will be adjusted such that the depth-averaged SPM concentration equals unity all the time: $[c] = 1$. The effect of the tidally oscillating motion is represented by the tidally varying bottom friction velocity u_*^b.

REFERENCES

Aiki, H., and R. J. Greatbatch, 2012: Thickness-weighted mean theory for the effect of surface gravity waves on mean flows in the upper ocean. *J. Phys. Oceanogr.*, **42**, 725–747, https://doi.org/10.1175/JPO-D-11-095.1.

——, and ——, 2013: The vertical structure of the surface wave radiation stress for circulation over a sloping bottom as given by thickness-weighted-mean theory. *J. Phys. Oceanogr.*, **43**, 149–164, https://doi.org/10.1175/JPO-D-12-059.1.

——, and ——, 2014: A new expression for the form stress term in the vertically Lagrangian mean framework for the effect of surface waves on the upper-ocean circulation. *J. Phys. Oceanogr.*, **44**, 3–23, https://doi.org/10.1175/JPO-D-12-0228.1.

Andrews, D. G., and M. E. McIntyre, 1978: An exact theory of nonlinear waves on a Lagrangian-mean flow. *J. Fluid Mech.*, **89**, 609–646, https://doi.org/10.1017/S0022112078002773.

Baumert, H., and G. Radach, 1992: Hysteresis of turbulent kinetic energy in nonrotational tidal flows: A model study. *J. Geophys. Res. Oceans*, **97**, 3669–3677, https://doi.org/10.1029/91JC02717.

Becherer, J., M. T. Stacey, L. Umlauf, and H. Burchard, 2015: Lateral circulation generates flood tide stratification and estuarine exchange flow in a curved tidal inlet. *J. Phys. Oceanogr.*, **45**, 638–656, https://doi.org/10.1175/JPO-D-14-0001.1.

——, G. Flöser, L. Umlauf, and H. Burchard, 2016: Estuarine circulation versus tidal pumping: Sediment transport in a

well-mixed tidal inlet. *J. Geophys. Res. Oceans*, **121**, 6251–6270, https://doi.org/10.1002/2016JC011640.

Burchard, H., 1999: Recalculation of surface slopes as forcing for numerical water column models of tidal flow. *Appl. Math. Modell.*, **23**, 737–755, https://doi.org/10.1016/S0307-904X(99)00008-6.

——, 2009: Combined effects of wind, tide, and horizontal density gradients on stratification in estuaries and coastal seas. *J. Phys. Oceanogr.*, **39**, 2117–2136, https://doi.org/10.1175/2009JPO4142.1.

——, and O. Petersen, 1997: Hybridization between σ- and z-co-ordinates for improving the internal pressure gradient calculation in marine models with steep bottom slopes. *Int. J. Numer. Methods Fluids*, **25**, 1003–1023, https://doi.org/10.1002/(SICI)1097-0363(19971115)25:9<1003::AID-FLD600>3.0.CO;2-E.

——, and K. Bolding, 2002: GETM—A General Estuarine Transport Model. Tech. Rep. EUR 20253 EN, JRC23237, European Commission, 157 pp., http://publications.jrc.ec.europa.eu/repository/bitstream/JRC23237/EUR%2020253%20EN.pdf.

——, and R. D. Hetland, 2010: Quantifying the contributions of tidal straining and gravitational circulation to residual circulation in periodically stratified tidal estuaries. *J. Phys. Oceanogr.*, **40**, 1243–1262, https://doi.org/10.1175/2010JPO4270.1.

——, H. M. Schuttelaars, and W. R. Geyer, 2013: Residual sediment fluxes in weakly-to-periodically stratified estuaries and tidal inlets. *J. Phys. Oceanogr.*, **43**, 1841–1861, https://doi.org/10.1175/JPO-D-12-0231.1.

——, and Coauthors, 2018: The Knudsen theorem and the Total Exchange Flow analysis framework applied to the Baltic Sea. *Prog. Oceanogr.*, **165**, 268–286, https://doi.org/10.1016/j.pocean.2018.04.004.

——, X. Lange, K. Klingbeil, and P. MacCready, 2019: Mixing estimates for estuaries. *J. Phys. Oceanogr.*, **49**, 631–648, https://doi.org/10.1175/JPO-D-18-0147.1.

Cheng, P., H. E. de Swart, and A. Valle-Levinson, 2013: Role of asymmetric tidal mixing in the subtidal dynamics of narrow estuaries. *J. Geophys. Res. Oceans*, **118**, 2623–2639, https://doi.org/10.1002/jgrc.20189.

de Szoeke, R. A., and A. F. Bennet, 1993: Microstructure fluxes across density surfaces. *J. Phys. Oceanogr.*, **23**, 2254–2264, https://doi.org/10.1175/1520-0485(1993)023<2254:MFADS>2.0.CO;2.

Dronkers, J., and J. van de Kreeke, 1986: Experimental determination of salt intrusion mechanisms in the Volkerak estuary. *Neth. J. Sea Res.*, **20**, 1–19, https://doi.org/10.1016/0077-7579(86)90056-6.

Giddings, S. N., S. G. Monismith, D. A. Fong, and M. T. Stacey, 2014: Using depth-normalized coordinates to examine mass transport residual circulation in estuaries with large tidal amplitude relative to the mean depth. *J. Phys. Oceanogr.*, **44**, 128–148, https://doi.org/10.1175/JPO-D-12-0201.1.

Greatbatch, R. J., and T. J. McDougall, 2003: The non-Boussinesq temporal residual mean. *J. Phys. Oceanogr.*, **33**, 1231–1239, https://doi.org/10.1175/1520-0485(2003)033<1231:TNTRM>2.0.CO;2.

Hansen, D. V., and M. Rattray Jr., 1965: Gravitational circulation in straits and estuaries. *J. Mar. Res.*, **23**, 104–122.

Hofmeister, R., H. Burchard, and J.-M. Beckers, 2010: Non-uniform adaptive vertical grids for 3D numerical ocean models. *Ocean Modell.*, **33**, 70–86, https://doi.org/10.1016/j.ocemod.2009.12.003.

Kasahara, A., 1974: Various vertical coordinate systems used for numerical weather prediction. *Mon. Wea. Rev.*, **102**, 509–522, https://doi.org/10.1175/1520-0493(1974)102<0509:VVCSUF>2.0.CO;2.

Kjerfve, B., 1975: Velocity averaging in estuaries characterized by a large tidal range to depth ratio. *Estuarine Coastal Mar. Sci.*, **3**, 311–323, https://doi.org/10.1016/0302-3524(75)90031-6.

Klingbeil, K., and H. Burchard, 2013: Implementation of a direct nonhydrostatic pressure gradient discretisation into a layered ocean model. *Ocean Modell.*, **65**, 64–77, https://doi.org/10.1016/j.ocemod.2013.02.002.

——, F. Lemarié, L. Debreu, and H. Burchard, 2018: The numerics of hydrostatic structured-grid coastal ocean models: State of the art and future perspectives. *Ocean Modell.*, **125**, 80–105, https://doi.org/10.1016/j.ocemod.2018.01.007.

Lerczak, J. A., W. R. Geyer, and R. J. Chant, 2006: Mechanisms driving the time-dependent salt flux in a partially stratified estuary. *J. Phys. Oceanogr.*, **36**, 2296–2311, https://doi.org/10.1175/JPO2959.1.

Longuet-Higgins, M. S., 1969: On the transport of mass by time-varying ocean currents. *Deep-Sea Res. Oceanogr. Abstr.*, **16**, 431–447, https://doi.org/10.1016/0011-7471(69)90031-X.

MacCready, P., 2011: Calculating estuarine exchange flow using isohaline coordinates. *J. Phys. Oceanogr.*, **41**, 1116–1124, https://doi.org/10.1175/2011JPO4517.1.

McDougall, T. J., and P. C. McIntosh, 2001: The temporal-residual-mean velocity. Part II: Isopycnal interpretation and the tracer and momentum equations. *J. Phys. Oceanogr.*, **31**, 1222–1246, https://doi.org/10.1175/1520-0485(2001)031<1222:TTRMVP>2.0.CO;2.

Simpson, J. H., J. Brown, J. Matthews, and G. Allen, 1990: Tidal straining, density currents, and stirring in the control of estuarine stratification. *Estuaries*, **13**, 125–132, https://doi.org/10.2307/1351581.

Stacey, M. T., J. P. Fram, and F. K. Chow, 2008: Role of tidally periodic density stratification in the creation of estuarine subtidal circulation. *J. Geophys. Res. Oceans*, **113**, C08016, https://doi.org/10.1029/2007JC004581.

Walin, G., 1977: A theoretical framework for the description of estuaries. *Tellus*, **29**, 128–136, https://doi.org/10.3402/tellusa.v29i2.11337.

Warner, J. C., C. R. Sherwood, H. G. Arango, and R. P. Signell, 2005: Performance of four turbulence closure models implemented using a generic length scale method. *Ocean Modell.*, **8**, 81–113, https://doi.org/10.1016/j.ocemod.2003.12.003.

Wolfe, C. L., 2014: Approximations to the ocean's residual circulation in arbitrary tracer coordinates. *Ocean Modell.*, **75**, 20–35, https://doi.org/10.1016/j.ocemod.2013.12.004.

Young, W. R., 2012: An exact thickness-weighted average formulation of the Boussinesq equations. *J. Phys. Oceanogr.*, **42**, 692–707, https://doi.org/10.1175/JPO-D-11-0102.1.

Zimmerman, J. T. F., 1979: On the Euler–Lagrange transformation and the Stokes' drift in the presence of oscillatory and residual currents. *Deep-Sea Res.*, **26A**, 505–520, https://doi.org/10.1016/0198-0149(79)90093-1.